2016 IEEE 55th Conference on Decision and Control (CDC)
ARIA Resort & Casino
December 12-14, 2016, Las Vegas, USA

Robust Acceleration Control of a Hexarotor UAV with a Disturbance Observer

Seung Jae Lee, Suseong Kim, Karl Henrik Johansson, and H. Jin Kim

Abstract— **This paper presents an acceleration control of a hexarotor unmanned aerial vehicle (UAV) in the earth-fixed frame with a disturbance observer (DOB). Unlike conventional cascade control structures where the outer-loop position controller generates the desired attitude command, the position controller in this paper generates the desired acceleration command in X, Y, Z axis of the earth-fixed frame. With acceleration control combined with DOB, the UAV could manage the lateral disturbance force that makes the trajectory tracking very challenging. This is a new concept compared with existing DOB-based UAV control approaches which aim to cancel the moment disturbance for precise attitude control. The small-gain theorem is used for stability analysis and Q-filter bandwidth design. Both simulation and actual experiment are shown to validate the performance of the proposed design.**

Index Terms - **Hexarotor, acceleration control, disturbance observer, small-gain theorem, robust position control.**

I. INTRODUCTION

Precise autonomous flight is an essential capability required for a wider application of UAVs (unmanned aerial vehicles). In particular, reliability against various types of unpredictable disturbance by which UAVs are constantly affected is an important issue in autonomous outdoor flight.

Despite various approaches used for attitude control that is commonly used as an inner loop of the cascade control structure for many UAVs [1], [2], [3], [4], their performance would significantly degrade when unmodeled dynamics exist or unwanted moments are generated due to the disturbance such as wind or gust since imprecise attitude control causes generation of inadequate force component toward each axis in earth-fixed frame. To address this issue, various types of disturbance observers have been applied to attitude controller of multirotor UAVs in [5], [6] and [7].

Still, DOB-applied attitude control is vulnerable to certain types of disturbances that act as a lateral force. Fig. 1 shows block diagrams representing channels through which the disturbance affects the system. In principle, DOB-applied attitude control considers the disturbance affecting the attitude control only (Fig. 1 (top)). However, in actual situation, lateral force disturbance affects the position control performance as illustrated in Fig. 1 (bottom). So, when the harsh lateral wind blows, even though the desired attitude is tracked with great performance, precise position control is nearly impossible. In this paper, we aim to develop a control algorithm to compensate lateral disturbance in the aspect of Fig. 1 (bottom). To accomplish this goal, we first develop an acceleration control method for X, Y, Z axis in the earth-fixed frame, which is an unique concept introduced in this paper to our best knowledge. As the lateral disturbance affects the UAV as a force, we need to control the total thrust and its fraction in each axis of an earth-fixed frame to overcome the disturbance force. After assembling the acceleration control, we apply a disturbance observer (DOB) algorithm. With DOB, we are able to estimate unwanted disturbance force by comparing the measurement of the resulting acceleration and calculated acceleration from the nominal transfer function of the UAV model. Then, by generating the desired acceleration command that can compensate the outer disturbance, we recover the nominal UAV dynamics.

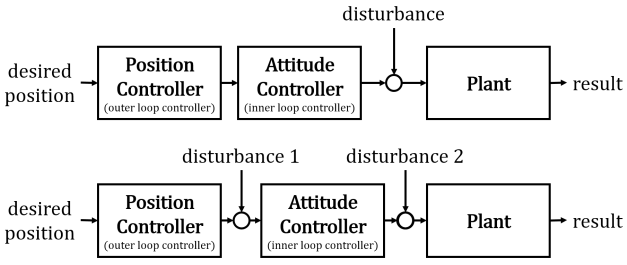

Fig. 1. Block diagram indicating each situation when outer disturbance interrupts attitude control only (top), both attitude and position control (bottom).

As mentioned above, there exist many references on how to manage the attitude disturbance with DOB [5], [6] and [7]. By using the attitude controller with DOB that rejects attitude disturbance, we can treat the attitude response as the nominal dynamics. This allows us to focus on the acceleration control with DOB as a mean of generating adequate acceleration while lateral disturbance is affecting the UAV dynamics. It first estimates unwanted external acceleration by comparing actual response with nominal model response, and generates a disturbance rejection signal as shown in Fig. 2.

This paper is organized as follows. In section II, the mathematical model of the UAV and problem solving approach will be covered. In section III, the proposed acceleration control method is derived. In section IV, the application of DOB in acceleration control is shown. Stability analysis of the system is shown in section V. Both simulation and the experimental results are shown in section VI.

Seung Jae Lee, Suseong Kim and H. Jin Kim are with the Department of Mechanical and Aerospace Engineering, Seoul National University, Gwanak-gu, Seoul, Korea sjlazza@snu.ac.kr, suseongkim@snu.ac.kr, hjinkim@snu.ac.kr

Karl Henrik Johansson is with the School of Electrical Engineering, KTH Royal Institute of Technology, Stockholm, Sweden kallej@kth.se

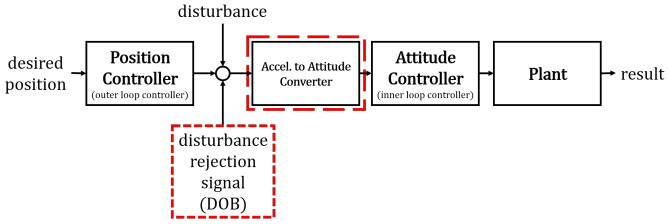

Fig. 2. Overall structure of the proposed DOB applied position controller

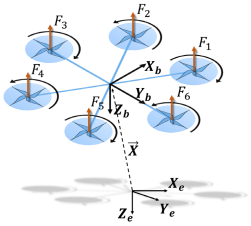

Fig. 3. Frame configuration of the hexarotor UAV

II. MODELLING OF A HEXAROTOR UAV

Before explaining the controller design, the kinematics and dynamics of the hexarotor are briefed in this section.

As shown in Fig. 3, a hexarotor is a multi-rotor UAV with six rotors rotating in opposite directions to neighbouring rotors. Six arms are implemented in 60 degree interval. All rotor's rotation axes are fixed to $\mathbf{Z_b}$ axis, making the propelling force heads toward $-\mathbf{Z_b}$ axis at all time. The pitch angle of the propeller is also fixed, resulting the propelling force and the generating moment that are related to the angular speed of the motor as

$$F_i = k\omega_i^2, \qquad M_i = b\omega_i^2 \tag{1}$$

where k is the rotor force constant, b is the rotor moment constant, and ω_i is a rotation speed of the motor i. F_i and M_i are the thrust and torque from the i-th motor respectively. Second, the rigid body dynamics of the UAV are given by

$$\begin{cases} m\ddot{\mathbf{x}} = R(\mathbf{q})T_f + mg\mathbf{Z_e} \\ J\dot{\mathbf{\Omega}} = T_m - \mathbf{\Omega} \times J\mathbf{\Omega} \end{cases} \tag{2}$$

where m is the mass of the UAV, J is the moment of inertia, $R(\mathbf{q})$ is the rotation matrix from the body frame to earth fixed frame, T_f is the thrust force vector in body frame with $T_f = [0\ 0\ -\Sigma F_i]^T$, T_m is the thrust torque vector in the body frame with $T_m = [\tau_r\ \tau_p\ \tau_y]^T$, and g is gravitational acceleration. The $\mathbf{x}$ is position in the earth fixed frame with $\mathbf{x} = [x\ y\ z]^T$, $\mathbf{q}$ is roll, pitch, yaw attitude angle in the earth-fixed frame with $\mathbf{q} = [\phi\ \theta\ \psi]^T$. $\mathbf{\Omega} = [p\ q\ r]^T$ is angular velocity in the body frame.[13].

The gyroscopic effect of the airframe is small that it is permissible to neglect the term $\mathbf{\Omega} \times J\mathbf{\Omega}$ in equation (2). The relationship between $\dot{\mathbf{q}}$ and Ω is

$$\dot{\mathbf{q}} = W(\mathbf{q})\Omega. \tag{3}$$

But when attitude angle is not big, the small angle assumption is valid, making $W(\mathbf{q}) \approx I_{3\times3}$. Since the roll and pitch angles of the hexarotor UAV during the flight are usually within 0.3 rad due to the structural reason, we can approximate $\dot{\mathbf{q}} \approx \Omega$ in a normal flight condition. The overall dynamics in equation (2) therefore can be rewritten as

$$\begin{cases} \ddot{x} = \frac{u_4}{m}(\cos\phi\sin\theta\cos\psi + \sin\phi\sin\psi) \\ \ddot{y} = \frac{u_4}{m}(\cos\phi\sin\theta\sin\psi - \sin\phi\cos\psi) \\ \ddot{z} = -\frac{u_4}{m}(\cos\phi\cos\theta) + g \end{cases} \quad \begin{cases} \ddot{\phi} = \frac{u_1}{J_{xx}} \\ \ddot{\theta} = \frac{u_2}{J_{yy}} \\ \ddot{\psi} = \frac{u_3}{J_{zz}}. \end{cases} \tag{4}$$

where u_1, u_2, u_3, u_4 are $\tau_r, \tau_p, \tau_y, \Sigma F_i$ respectively that are applied to the airframe.

III. ACCELERATION CONTROL

For acceleration control in the earth-fixed frame, we look back at the dynamics of the system. The relationship between acceleration in the earth fixed frame and control states of UAV is shown in the first three equations of equation (4), which can be organized as

$$\ddot{\mathbf{x}} = G(\mathbf{q}, u_4)\mathbf{r} + g\mathbf{Z_e} \tag{5}$$

where $\mathbf{r} = [\phi\ \theta\ \Sigma F_i]^T$ is the control signal, and $G(\mathbf{q}, u_4)$ the relationship between $\ddot{\mathbf{x}}$ and $\mathbf{r}$. The yaw state is controlled by a separate controller. For derivation of $G(\mathbf{q}, u_4)$, we apply a small angle assumption to the trigonometric functions of roll and pitch angles since these angles are less than 0.3 rad. Then the first two equations of equation (4) become

$$\begin{cases} \ddot{x} = \frac{u_4}{m}(\theta\cos\psi + \phi\sin\psi) \\ \ddot{y} = \frac{u_4}{m}(\theta\sin\psi - \phi\cos\psi) \end{cases}. \tag{6}$$

With these equations, equation (5) can be written as

$$\begin{bmatrix} \ddot{x} \\ \ddot{y} \\ \ddot{z} \end{bmatrix} = \begin{bmatrix} \frac{u_4}{m}s\psi & \frac{u_4}{m}c\psi & 0 \\ -\frac{u_4}{m}c\psi & \frac{u_4}{m}s\psi & 0 \\ 0 & 0 & \frac{-1}{m}c\phi c\theta \end{bmatrix} \begin{bmatrix} \phi \\ \theta \\ \Sigma F_i \end{bmatrix} + \begin{bmatrix} 0 \\ 0 \\ g \end{bmatrix} \tag{7}$$

where symbols $s\phi$ and $c\phi$ stand for $\sin\phi$ and $\cos\phi$.

Now, if we want to control the acceleration of the UAV (i.e., $\ddot{\mathbf{x}}$), we need equation (5) to convert the desired acceleration $\ddot{\mathbf{x}}_d$ to the desired control signal $\mathbf{r}_d$. Such $\mathbf{r}_d$ is calculated as

$$\mathbf{r}_d = G^{-1}(\mathbf{q}, u_4)(\ddot{\mathbf{x}}_d - g\mathbf{Z_e}). \tag{8}$$

One problem in this formula is that we cannot achieve the magnitude of u_4 the current thrust, because measuring the net force of the rotors during the flight is very hard. So we have to calculate u_4 using the remaining measurable states.

In equation (2), the total force applied to the UAV in the sense of earth-fixed frame is $R(\mathbf{q})T_f + [0\ 0\ mg]^T$. T_f can be written as $[0\ 0\ -u_4]^T$. So, we can write this relationship as

$$\begin{bmatrix} 0 \\ 0 \\ u_4 \end{bmatrix} = -mR^{-1}(\mathbf{q}) \begin{bmatrix} a_x \\ a_y \\ a_z - g \end{bmatrix}. \tag{9}$$

We can see that the components used to calculate u_4 are $m, \mathbf{q}, a_x, a_y, a_z$. The mass is pre-known and the other terms can be measured using an inertial navigation sensor. So with equation (9), we can calculate u_4.

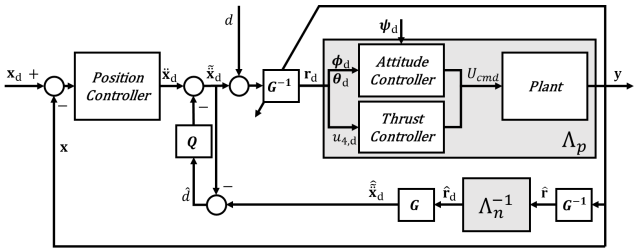

Fig. 4. Detailed overall control scheme with acceleration DOB

IV. DISTURBANCE OBSERVER

In this section, we will show a strategy to control acceleration of UAV in earth-fixed frame even with certain amount of disturbance force is applied to the airframe. Since the focus of this paper is to minimize the effect of the disturbance affecting the position control as denoted as 'disturbance 1' in Fig. 1 (bottom), we assume that the nominal attitude dynamics of UAV is not disturbed by the outer disturbance in order to simplify the discussion. This assumption is valid when we implement an attitude DOB to the attitude controller so that it could behave as a nominal system [6]. This allows us to only care about the disturbance affecting the acceleration control in the earth-fixed frame.

A. Overall Control Scheme

The cascade control loop is considered for position control of the UAV as shown in Fig. 4. The position controller that acts as an outer loop controller generates $\ddot{\mathbf{x}}_d$. Then, $G^{-1}(\mathbf{q}, u_4)$ matrix converts $\ddot{\mathbf{x}}_d$ to $\mathbf{r}_d$ where $\mathbf{r}_d = [\phi_d, \theta_d, u_{4,d}]^T$. The attitude controller generates $\tau_{roll}, \tau_{pitch}, \tau_{yaw}$ signal that makes platform to follow $\mathbf{r}_d$.

The signal ψ_d is provided to the attitude controller in a separate manner as shown in Fig. 4. The thrust controller generates a control signal that makes u_4 to follow $u_{4,d}$. Therefore, the airframe behaves with generated commands under dynamic constraints in equation (2). When there is no disturbance, the airframe behaves like the nominal system. But with exogenous disturbance, the system behaves differently.

B. Disturbance Observer

This subsection describes the DOB algorithm applied to the acceleration control. The disturbance in Fig. 4 is symbolized as d. Main idea of the disturbance observer is to estimate the value d and compensate it in the next step of control. In order to estimate d, first we have to define the nominal transfer function of the gray box that consists of the hexarotor plant with attitude and thrust controllers, marked as Λ_p in Fig. 4. It is the transfer function between $\mathbf{r}_d$ and $\mathbf{y}$ with $\mathbf{y} = \Lambda_p \mathbf{r}_d$. We cannot find Λ_p in reality, but we can find the nominal transfer function Λ_n. With Λ_n, we can calculate the estimated control input $\hat{\mathbf{r}}_d$ with $\hat{\mathbf{r}}_d = \Lambda_n^{-1}\hat{\mathbf{r}}$, which $\hat{\mathbf{r}}$ represents an estimated attitude of the UAV based on current lateral acceleration. Then multiplication of the G matrix in equation (5) transforms $\hat{\mathbf{r}}_d$ into $\hat{\tilde{\ddot{\mathbf{x}}}}_d$, which is an estimated value of $\tilde{\ddot{\mathbf{x}}}_d$ in Fig. 4. The symbol $\hat{*}$ represents the estimated quantity throughout this paper. The estimation of d is done by

$$\hat{d} = \hat{\tilde{\ddot{\mathbf{x}}}}_d - \tilde{\ddot{\mathbf{x}}}_d. \tag{10}$$

The nominal model Λ_n used to calculate $\hat{r}_d$ is a minimum-phase, linear time-invariant system whose relative degree is grater than 1. So, ${\Lambda_n}^{-1}$ becomes an improper function that violates causality. To suppress it, we use a Q-filter, which makes the overall transfer function proper. When Λ_n has relative degree r, the Q-filter is generally designed as

$$Q(s) = \frac{b_k(\tau s)^k + b_{k-1}(\tau s)^{k-1} + \cdots + b_0}{(\tau s)^l + a_{l-1}(\tau s)^{l-1} + \cdots + a_1(\tau s) + a_0} \tag{11}$$

where $l \geq k + r$ and $b_0 = a_0$ so the value of Q is 1 when $s = 0$ [8].

The nominal transfer function Λ_n is constructed from two parts: attitude control and thrust control. We denote these as $\Lambda_{n,a}$ and $\Lambda_{n,t}$ respectively. In order to derive $\Lambda_{n,a}$, we should look back at equation (2). In equation (2), the attitude dynamics of the UAV is composed of the inertial moment term $J\mathbf{\Omega}$ and the gyroscopic effect term $\mathbf{\Omega} \times J\mathbf{\Omega}$. As mentioned, the gyroscopic effect is so small compared to the inertial moment term in common multirotor UAVs that we can simply neglect it. Rewriting it, the attitude dynamics with implication of $\dot{\mathbf{q}} = \Omega$ is

$$T_m = J\dot{\Omega} = J\ddot{\mathbf{q}}. \tag{12}$$

So, the transfer function between T_m and $\mathbf{q}$ is

$$\frac{\mathbf{q}_i(s)}{T_{m,i}(s)} = \frac{1}{J_{ii}s^2} \tag{13}$$

where $i = 1, 2, 3$ represents ϕ, θ, ψ respectively. The J_{ii} is $(i,i)^{th}$ component of J matrix.

PID control is used for the attitude controller. The transfer function $\Lambda_{n,a,i}(s)$, i.e. the relationship between desired and current attitude with consideration of the controller for each attitude angle, is therefore

$$\begin{cases} \frac{\mathbf{q}_i(s)}{\mathbf{q}_{d,i}(s) - \mathbf{q}_i(s)} = \frac{P_i s + I_i + D_i s^2}{s} \frac{1}{J_{ii}s^2} \\ \Lambda_{n,a,i}(s) = \frac{\mathbf{q}_i(s)}{\mathbf{q}_{d,i}(s)} = \frac{D_i s^2 + P_i s + I_i}{J_{ii}s^3 + D_i s^2 + P_i s + I_i} \end{cases} \tag{14}$$

where P_i, I_i, D_i represent PID gains of the attitude controller. The transfer function $\Lambda_{n,t}$ between $u_{4,d}$ and $u_{4,c}$, with $u_{4,d} = \Lambda_{n,t} u_4$, should include rotor dynamics and the electronic controller unit (ECU) response. But in normal situations, thrust response could be modelled as a time delay model. So, the nominal transfer function of the PID controlled thrust $\Lambda_{n,t}$ is

$$\begin{cases} \frac{u_{4,c}(s)}{u_{4,d}(s) - u_{4,c}(s)} = \frac{P_t s + I_t + D_t s^2}{s} \frac{1}{T_{th}^2 s^2 + 2\zeta T_{th} s + 1} \\ \Lambda_{n,t} = \frac{u_{4,c}(s)}{u_{4,d}} = \frac{D_t s^2 + P_t s + I}{T_{th}^2 s^3 + (2\zeta T_{th} + D_t)s^2 + (P_t + 1)s + I_t} \end{cases} \tag{15}$$

where P_t, I_t, D_t are PID gains in the thrust controller and T_{th} is a variable to mimic the time gap between $u_{4,d}$ and $u_{4,c}$[10].

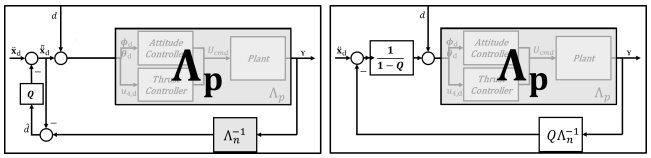

Fig. 5. Simplified structure (left) and equivalent single feedback loop (right) of overall control scheme

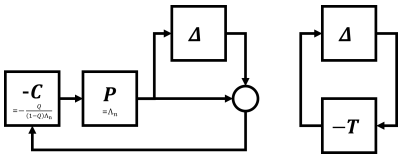

Fig. 6. Block diagram with P and C(left), filled form of P and C block(middle), equivalent form(right)

V. STABILITY ANALYSIS

Before starting the stability analysis of the proposed control algorithm, we assume that heading angle ψ holds zero during the flight. It is to simplify the proof by considering roll and pitch movement related to $\ddot{x}, \ddot{y}$ independently.

In this section, we are going to find the boundary of the tunable parameters, especially the bandwidth of the Q-filter to guarantee the stability of the system.

A. Small Gain Theorem

The reason of the difference between the nominal plant Λ_n and the actual plant Λ_p can be attributed to two factors: modelling error and time delay. In this paper, we consider the constant time delay only. If we represent the nominal plant model as

$$\Lambda_n(s) = \frac{B_n(s)}{A_n(s)} \tag{16}$$

the actual plant model could be written as

$$\Lambda_p(s) = e^{-sT_d}\frac{B_n(s)}{A_n(s)} \tag{17}$$

where T_d is the time delay between the nominal model and actual plants [8]. The major issue in ensuring the stability of the system is $Q(s)$, whose bandwidth controls the balance between the disturbance rejection performance and the stabilization performance.

Fig. 5 shows the simplified and equivalent structure of Fig. 4. Unlike Fig. 4, the structure in the right of Fig. 5 is causal. Based on Fig. 5(right), T_1 the transfer function between command and y and T_2 the transfer function between disturbance and y are as

$$T_1(s) = \frac{\Lambda_p(s)\Lambda_n(s)}{\Lambda_n(s) + Q(s)(\Lambda_p(s) - \Lambda_n(s))} \tag{18}$$

$$T_2(s) = \frac{\Lambda_p(s)\Lambda_n(s)(1 - Q(s))}{\Lambda_n(s) + Q(s)(\Lambda_p(s) - \Lambda_n(s))}. \tag{19}$$

When the input frequency is low, $Q(s)$ should become approximately 1, making $T_1 \approx \Lambda_n(s)$ and $T_2 \approx 0$ as $Q(s) \approx 1$. Because of this requirement, the $Q(s)$ filter should be a low pass filter.

Equations (16) and (17) can be written as

$$\Lambda_p(s) = e^{-sT_d}\Lambda_n(s), \tag{20}$$

which leads to the following multiplicative perturbation form

$$\Lambda_p(s) = \Lambda_n(s)(1 + \Delta(s)) \tag{21}$$

with

$$\Delta(s) = e^{-s_d} - 1. \tag{22}$$

The block diagram with the multiplicative perturbation model is in Fig. 6. Matching the structure with Fig. 5(right), we can derive that C and P blocks in Fig. 6(left) as $-\frac{Q}{(1-Q)\Lambda_n}$ and Λ_n respectively. It can be simplified further with only two blocks as shown in Fig. 5(right). The complimentary sensitivity function T can be calculated as

$$T = \frac{PC}{1 + PC} = \frac{\Lambda_n \frac{Q}{(1-Q)\Lambda_n}}{1 + \Lambda_n \frac{Q}{(1-Q)\Lambda_n}} = Q. \tag{23}$$

The stability of the system with the structure in Fig. 5(right) is guaranteed by the small gain theorem [11]:

$$||\Delta \cdot T||_\infty = ||\Delta \cdot Q||_\infty < 1. \tag{24}$$

The term Δ in equation (22) is a fixed transfer function that only depends on the hardware specification. So, by tuning Q filter, we can make this inequality proper.

B. Q-filter Design

Since the nominal transfer function has been set by $\Lambda_{n,a}$ and $\Lambda_{n,t}$, we will find an adequate τ value in the Q filter to satisfy equation (24). The parameters in Q are a_0, a_1, τ. We set a_0, a_1 to 1 and 2 respectively with discretion. Then, the only tunable parameter is τ.

The time delay between nominal plant and real plant T_d is computed by measuring the time delay between desired and real plant responses (T_p) and the time delay between desired and nominal plant responses (T_n) and subtracting them :

$$T_d = T_p - T_n. \tag{25}$$

T_n can be measured by the comparison between input and output response of Λ_n in simulation results. The time delay $T_{n,a}$ of $\Lambda_{n,a}$ has been measured to be approximately 0.3 seconds and $T_{n,t}$ of $\Lambda_{n,t}$ approximately 0.1 seconds with observation of simulation results. Similarly time delays $T_{p,a}$ and $T_{p,t}$ of Λ_p can be measured, which are approximately 0.4 seconds and 0.2 seconds. With the equation (25), we then find $T_{d,a}$ and $T_{d,t}$ to be both near 0.1 seconds. Thus, we have

$$\Delta = e^{-0.1s} - 1. \tag{26}$$

Based on equation (24), the stability of the system is guaranteed when we satisfy the equation below.

$$||Q(s)||_\infty < \frac{1}{||\Delta(s)||_\infty} \tag{27}$$

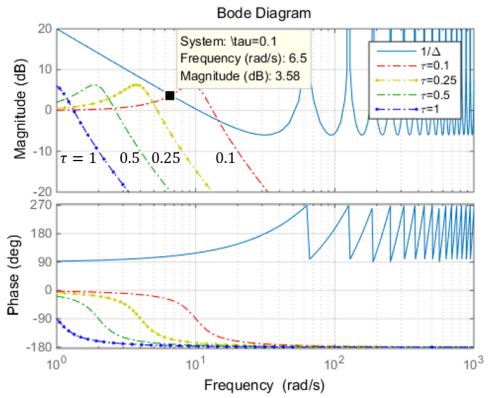

Fig. 7. Bode diagram of Λ^{-1} and Q with various τ values

Fig. 7 shows the Bode diagram of $\Delta^{-1}(s)$ and $Q(s)$ with variable τ values. The blue solid graph on the upper side of the plot is $\Delta^{-1}(s)$ and another four graphs are Q-filter plot with various τ values. In Fig 7, when $\tau = 0.1$, we can see that the $Q(s)$ curve intrudes the $\Delta^{-1}(s)$ graph in the frequency range from 6.5 rad/s. This means that, when DOB with $\tau = 0.1$ faces disturbances with that frequency range, the system could fail. But Q plot with τ bigger than 0.25 does not intrude $\Delta^{-1}(s)$ curve. Although the T_d value is found empirically and it makes hard to find the exact smallest value of τ, but we can say that the suitable range is within 0.1 to 0.25. A higher τ value makes the system stable but causes poor disturbance rejection. So we set τ in $\Lambda_{p,a}$ as $\tau = 0.25$.

VI. SIMULATION AND EXPERIMENT

In this section, the simulation and experimental results of the autonomous flight of UAV with an outer disturbance are reported. The comparison of trajectory tracking performance between with and without DOB is shown both in simulation and experiment.

A. Simulation Result

A UAV in the simulation follows a 3-m radius circular path at the altitude of 5-m, subject to the periodic disturbance with the amplitude upto 5.5 m/s^2.

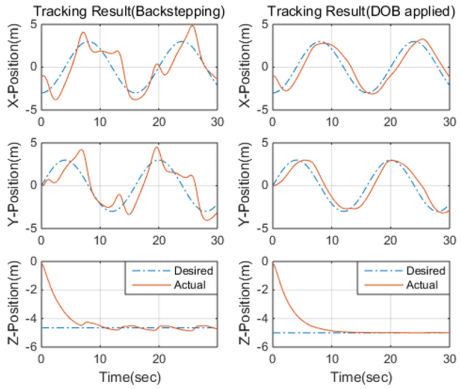

Fig. 8. Trajectory tracking result with backstepping position control (left), PID position control with DOB applied (right). [Simulation Result]

Fig. 8(left) shows the simulation result of the UAV controlled by a backstepping controller [12]. As we can see, the trajectory tracking performance is poor because disturbance interrupted the lateral control. Meanwhile, the trajectory tracking of UAV using DOB with a basic PID controller shows much improved performance as shown in Fig. 8(right).

We can see in Fig. 9(left) that there is a difference between $\ddot{x}_d$ (dashed) and $\tilde{\ddot{x}}_d$ (solid), i.e., the desired acceleration command coming from the position controller and the signal compensated by DOB respectively. Unlike the original command, the DOB-compensated signal $\tilde{\ddot{x}}_d$ became enlarged in order to compensate the lateral disturbance force. It means that the additional acceleration command is used to cancel the disturbance. Fig. 9(right) shows the actual disturbance d (unknown to the DOB and controller) and the estimated disturbance $\hat{d}$. The estimated disturbance value oscillates at first due to the different initial value from the true value. But within two seconds it converges and estimates well. The estimated disturbance is then added to the acceleration command and it compensates the outer disturbance for UAV to behave with the desired acceleration.

B. Experimental Result

In the experiment, a disturbance force is applied by pulling a tether attached to the airframe, and the position holding capability is measured. As shown in Fig. 11, the operator holds the tether attached to the airframe and pulls it to apply the disturbance force in one direction. Meanwhile, the load cell attached to another end of the tether measures the tension of the tether so that we can compare the estimated disturbance and applied disturbance force. Then comparison of the position tracking performance is made between the PID-only controller and DOB-applied controller.

Fig. 10 shows the desired position tracking result of the PID-only (left) and DOB-applied situation (right), under the disturbance applied in the X-axial direction. We can see that the DOB-applied case remains near the desired position, when compared with the PID-only case. Fig. 12(top) shows an overlapped plot of $\ddot{\mathbf{x}}_d$ (the acceleration command before DOB is applied) and $\tilde{\ddot{\mathbf{x}}}$ (the acceleration command after DOB

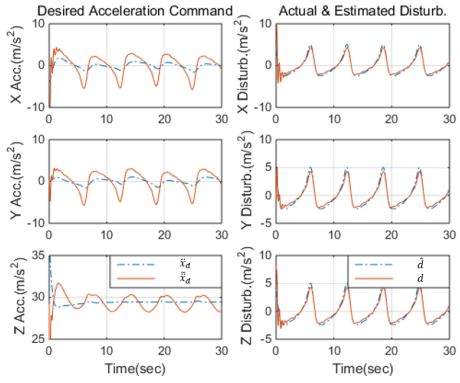

Fig. 9. Acceleration command before (dashed) and after (solid) the DOB is applied (left), actual and estimated disturbance by the proposed DOB structure (right). [Simulation Result]

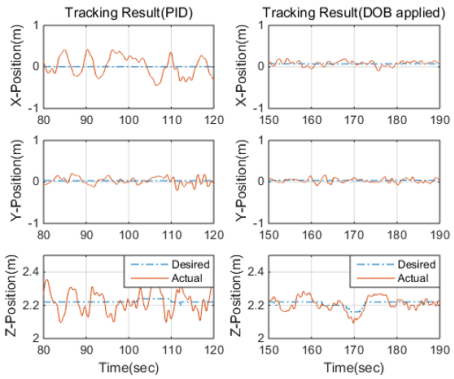

Fig. 10. Trajectory tracking result with PID-only position control (left), DOB applied control result (right).[Experimental Result]

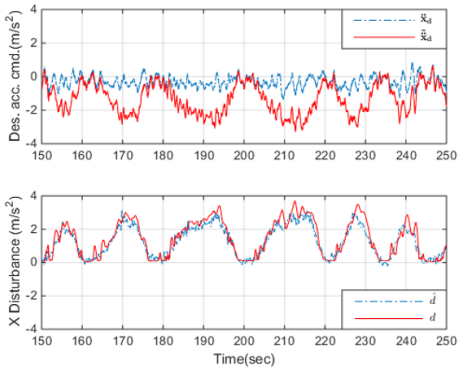

Fig. 12. Acceleration command before and after DOB applied (top), actual and measured disturbance (bottom).[Experimental Result]

is applied). As we can see, $\tilde{\ddot{x}}$ is biased toward the negative X-axial direction since the disturbance applied by the tether is in the positive X direction. The snapshot in Fig. 11 shows that the UAV's attitude is tilted to the opposite direction of the tether-pulling direction while the UAV keeps the desired position, which is to generate the compensation thrust. Fig. 12(bottom) confirms good agreement between $\hat{d}$, i.e., the estimated disturbance computed in on-board computer, and the measured disturbance by load cell. Since the disturbance is estimated from the acceleration data measured by IMU, the unit of disturbance in this plot is m/s^2, which can be easily converted to force by multiplying the mass of the UAV. Overall, this experiment demonstrates the position control performance of the proposed control structure under the force disturbance.

VII. CONCLUSIONS

In this work, the position control method that has an ability to compensate the unwanted disturbance is proposed. In particular, for the rejection of the force disturbance, a new acceleration control structure is designed. Using a disturbance observer, the estimation and rejection of the disturbance is accomplished. The stability of the algorithm was analyzed by the small gain theorem, with which the minimal bandwidth value of the Q filter for ensuring the stability of the system is also calculated. Both simulation and actual experiment are performed, from which we confirm that the proposed algorithm is an effective method for disturbance rejection.

Fig. 11. Experimental set-up of a DOB-applied UAV with an elastic tether to apply an outer lateral disturbance and a load cell to measure the disturbance force.

ACKNOWLEDGEMENTS

This research was supported by the National Research Foundation of Korea (NRF) grant funded by the Korean government (MSIP) (2014R1A2A1A12067588) and the Technology Innovation Program (10051673) funded by the Ministry of Trade, Industry & Energy (MI, Korea).

REFERENCES

[1] Yun, Yu, et al. "High performance full attitude control of a quadrotor on SO (3)." Robotics and Automation (ICRA), 2015 IEEE International Conference on. IEEE, 2015.

[2] Liu, Hao, Xiafu Wang, and Yisheng Zhong. "Quaternion-based robust attitude control for uncertain robotic quadrotors." Industrial Informatics, IEEE Transactions on 11.2 (2015): 406-415.

[3] Bouabdallah, Samir, and Roland Siegwart. "Backstepping and sliding-mode techniques applied to an indoor micro quadrotor." Robotics and Automation, 2005. ICRA 2005. Proceedings of the 2005 IEEE International Conference on. IEEE, 2005.

[4] Alexis, Kostas, George Nikolakopoulos, and Anthony Tzes. "Switching model predictive attitude control for a quadrotor helicopter subject to atmospheric disturbances." Control Engineering Practice 19.10 (2011): 1195-1207.

[5] Wang, Honglin, and Mou Chen. "Trajectory tracking control for an indoor quadrotor UAV based on the disturbance observer." Transactions of the Institute of Measurement and Control (2015): 0142331215597057.

[6] Lee, Kooksun, Juhoon Back, and Ick Choy. "Nonlinear disturbance observer based robust attitude tracking controller for quadrotor UAVs." International Journal of Control, Automation and Systems 12.6 (2014): 1266-1275.

[7] Besnard, Lnack, Yuri B. Shtessel, and Brian Landrum. "Quadrotor vehicle control via sliding mode controller driven by sliding mode disturbance observer." Journal of the Franklin Institute 349.2 (2012): 658-684.

[8] Kempf, Carl J., and Seiichi Kobayashi. "Disturbance observer and feedforward design for a high-speed direct-drive positioning table." Control Systems Technology, IEEE Transactions on 7.5 (1999): 513-526.

[9] Bhattacharyya, S. P., H. Chapellat, and L. H. Keel. "Robust control: the parametric approach." Upper Saddle River (1995).

[10] Nilsson, Johan. "Real-time control systems with delays." Department of Automatic Control, Lund Institute of Technology 1049 (1998).

[11] Jiang, Z-P., Andrew R. Teel, and Laurent Praly. "Small-gain theorem for ISS systems and applications." Mathematics of Control, Signals and Systems 7.2 (1994): 95-120.

[12] Adigbli, Patrick, et al. "Nonlinear attitude and position control of a micro quadrotor using sliding mode and backstepping techniques." (2007).

[13] Hoffmann, Gabriel M., et al. "Quadrotor helicopter flight dynamics and control: Theory and experiment." Proc. of the AIAA Guidance, Navigation, and Control Conference. Vol. 2. 2007.